J Mater Sci (2010) 45:6763–6768
DOI 10.1007/s10853-010-4772-1

Interface roughness influence on exchange bias effect in $La_{2/3}Ca_{1/3}MnO_3/La_{1/3}Ca_{2/3}MnO_3$ bilayers

E. Restrepo-Parra · G. Orozco-Hernández · J. Urrea-Serna · J. F. Jurado · J. C. Vargas-Hernández · J. C. Riaño-Rojas · J. Restrepo

Received: 30 November 2009 / Accepted: 15 July 2010 / Published online: 4 August 2010

Abstract A Monte Carlo simulation study of $La_{2/3}Ca_{1/3}MnO_3/La_{1/3}Ca_{2/3}MnO_3$ bilayers exchange bias (EB) properties by using a classical Heisenberg model and Monte Carlo method with Metropolis algorithm is addressed. Samples were built atom-by-atom in order to resemble the real roughness. In this model, several contributions included nearest neighbors exchange interactions; two different interface couplings, magnetocrystalline anisotropy and Zeeman term, were considered. Here, an influence of the relaxation steps on the interface roughness is present. Our study focuses on the influence of interface roughness on hysteresis loops, particularly EB field (H_{ex}) and coercive force (H_c). Results reveal that H_{ex} and H_c decrease as the interface roughness increases.

Introduction

Three factors generally influence the materials quality and functionality in technological applications: chemical composition, morphology (bulk structure; form, size, and shape), and surface topography (spatial relation of surface features). Although these aspects may be considered as being of equal importance, the materials technological performance in several fields as heat transfer between solid bodies, optics, electrical transport, tribology (wear and lubrication), adhesion, wetting, biocompatibility and magnetism is often strongly dependent on surface topography and roughness [1–4]. Regarding to magnetic properties, surface and interface roughness influence magnetic anisotropy, coercivity, magnetic domain structure, and magnetoresistance among others [5]. This influence is higher in the case of thin films that is associated with deposition methods, which have a direct effect on the solid-thin film devices behavior [6]. One of the most important effects in magnetic thin films specially grown as ferromagnetic/antiferromagnetic bilayers is the exchange bias (EB). This effect arises from magnetic coupling at the FM/AF interfaces, and is normally observed when a sample is cooled under an applied magnetic field from a temperature T lower than Curie temperature (T_c) but higher than the AF Néel temperature (T_N). EB is characterized by a shift of the magnetic hysteresis loop along the magnetic field axis. In fact, the EB effect can be established either by field cooling the FM/AF bilayer from temperatures above the AF T_N or by film deposition under an external magnetic field. Since its discovery, the EB effect has been much investigated and has found many technological applications [7–9] such as giant magneto-resistive spin valves and magnetic memory devices [10]. Because it is an interlayer phenomenon, it is well known that the magnitude of EB field in bilayers and multilayers depends on various factors like roughness between the FM and AF materials, textures (structural and magnetic), crystalline grain size, and AF layer thickness [11]. Nevertheless, the roughness

E. Restrepo-Parra (✉) · G. Orozco-Hernández · J. Urrea-Serna · J. F. Jurado · J. C. Vargas-Hernández
Departamento de Física y Química, Universidad Nacional de Colombia-Sede Manizales, A.A. 127, Manizales, Colombia
e-mail: erestrepopa@unal.edu.co

J. C. Riaño-Rojas
Departamento de Matemáticas y Estadística, Universidad Nacional de Colombia-Sede Manizales, A.A. 127, Manizales, Colombia

J. Restrepo
Grupo de Magnetismo y Simulación G, Instituto de Física, Universidad de Antioquia, A.A. 1226, Medellín, Colombia

dependence of EB is still dubious in the literature. For several magnetic systems, the H_{ex} magnitude is inversely proportional to the roughness value [12–15], while in other cases the opposite behavior has been reported [16]. There are also systems that seem to be almost insensitive to the roughness effect [17]. The $La_{2/3}Ca_{1/3}MnO_3/La_{1/3}Ca_{2/3}MnO_3$ exchange-biased system was extensively studied in the last decades especially in experimental way, basically due to its high H_{ex} and low coercive field (H_c) values, which enhance its potential for application in magnetic sensors. For instance, literature report studies of FM-LCMO and AF-LCMO multilayers, produced experimentally, analyzing the EB mechanisms [18, 19]. Nevertheless no enough studies of interface roughness influence on magnetic properties have been carried out.

The aim of this study is to analyze the interface roughness influence on EB field and coercive force in $La_{2/3}Ca_{1/3}MnO_3/La_{1/3}Ca_{2/3}MnO_3$ bilayers. The grown process atom-by-atom was simulated and then the hysteresis loops were obtained, and magnetic features as EB and coercive fields were determined.

Model description

The manganite $La_{2/3}Ca_{1/3}MnO_3$ is characterized for having three types of magnetic ions corresponding to Mn^{4+} ($S = 3/2$), which are bonded to Ca^{2+} ions, Mn^{3+eg} and $Mn^{3+eg'}$ ($S = 2$) that are related to La^{3+}. The five d orbitals of transition metallic ions with octahedral coordination can be divided in two sets: two orbitals with their lobules pointed toward the neighbor oxygen ions eg and eg'. The electrons placed in these orbitals are normally named unlocalized electrons. The other three orbitals with nodal planes in these directions are usually named t_{2g} and the electrons in these orbitals are considered as localized electrons [20]. Mn ions orbital ordering is implemented according to it proposed by Hotta et al. [21, 22]. In order to build the interface roughness, Monte Carlo method was used for simulating growth. The films growth requires the inclusion of both deposition and diffusion processes. Some efforts have been directed at fully understanding the behavior of relatively realistic models for small films using empirical potentials for short times, and other studies have been directed at the scaling behavior of simpler models. This realistic model approach is also in terms of solid on solid models with nearest neighbor interactions, which considers more realistic form of the microscopic potential of the ion–ion interaction in the grown process [23]. Particles are deposited with some fixed flux F this flux consists in sending a pulse of $L \times L$ atoms each time. After each pulse, any of the particles may then undergo activated diffusion with probability

$$p = \exp(-\Delta E/k_B T) \tag{1}$$

where ΔE is the energy difference between an initial state and other state generated randomly. k_B is the Boltzmann constant, and T is the temperature. For simple models with nearest neighbor coupling, the energy is simply dependent upon the number of occupied nearest neighbors, i.e., $E = \sum n_i$, being n_i the nearest neighbors of the ith ion. An atom that should be moved has to fulfill the requirement of being a surface ion. Then it can hops to a nearest neighbor site either randomly or with a probability which depends upon the energy that the atom will have in that site. Thus, the rate of hopping depends merely upon the relative energies of the configuration before and after hopping. The nature of the growth depends upon the magnitude of the flux as well as the temperature, detaching incident angle, resputtering effect, roughness cumulative process, and atmosphere blocking, which are not considered in our model. The growth process may be repeated multiple times with different random number sequences [24] and with the possibility of varying the number of pulses. Periodic boundary conditions in the x–y plane and free boundary conditions in z-directions were implemented and the model employed is based on a three-dimensional classical Heisenberg Hamiltonian including terms of exchange coupling between magnetic nearest neighbors, single-ion site surface anisotropy, cubic magnetocrystalline anisotropy for core ions, and a Zeeman term accounting for the interaction of the spins with an uniform external applied magnetic field [25]. Magnetic ions $Mn^{3+eg'}$, Mn^{3+eg}, and Mn^{4+d3} are represented by classical Heisenberg spins with different magnitudes according to their corresponding electronic configurations. Oxygen, calcium, and lanthanum ions are considered as non-magnetic. The Hamiltonian describing the interactions in our system reads as follows

$$\begin{aligned} H = & -J_F \sum_{i \neq j \in FM} \vec{S}_i \cdot \vec{S}_j - K_F \sum_{i \in FM} (\vec{S}_i \cdot \hat{a}_{FM})^2 \\ & - J_A \sum_{i \neq j \in AF} \vec{S}_i \cdot \vec{S}_j - K_A \sum_{i \in AF} (\vec{S}_i \cdot \hat{a}_{AF})^2 \\ & - J_{FA1} \sum_{i \neq j \in inter} \vec{S}_i \cdot \vec{S}_j - J_{FA2} \sum_{i \neq j \in inter} \vec{S}_i \cdot \vec{S}_j \\ & - h \sum_i \vec{S}_i \cdot \hat{h} \end{aligned} \tag{2}$$

where S_i and S_j are classical Heisenberg spin vectors. The first and third sums run over nearest neighbors pairs of spins coupled through exchange interactions $J_{FM} > 0$ for the FM layer and $J_{AF} < 0$ for the AF layer. Exchange mechanisms for FM and AF phases are different. Metallic ferromagnetism in the mixed valence manganites of perovskite structure, such as $La_{1-x}Ca_xMnO_3$, can be understood by Zener's double-exchange mechanism [26].

Recently, Bao et al. [27] carried out experimental studies supporting the view that there are only two important generic states in these manganites. In one on them, the charge carriers are mobile and the magnetism is determined by the double-exchange mechanism which supports ferromagnetic correlations. In the other state, the charge carriers are localized on the lattice and the magnetism is determined by the super-exchange which supports antiferromagnetic correlations.

For the FM layer, three types of bonds with their corresponding superexchange parameters were considered: $Mn^{3+eg'}$–O–Mn^{3+eg} (4.65 meV), Mn^{3+eg}–O–Mn^{4+d3} (7.7 meV), and $Mn^{3+eg'}$–O–Mn^{4+d3} (1.35 meV) [23]. In the case of AF layer, four parameters were used: $Mn^{3+eg'}$–O–Mn^{3+eg} (9.3 meV), Mn^{3+eg}–O–Mn^{4+d3} (15.54 meV), $Mn^{3+eg'}$–O–Mn^{4+d3} (2.7 meV), and Mn^{4+d3}–O–Mn^{4+d3} (8.6 meV). Parameters for FM layer were reported in a previous work [28], while first three constants for AF layer are twice FM parameters. The last interaction that normally does not appear in the FM layer was fitted for pure $CaMnO_3$ (which only contains Mn^{4+d3} ions), in order to reproduce the transition temperature ($\sim$140 K) under bulk conditions. Fifth and sixth terms account for the interaction between the FM and the AF layers and J_{FA1} and J_{FA2} are the corresponding alternated exchange constants at the interface and they constitute a novel mechanism to break the spatial reversal symmetry required to generate EB [29], in this study, they are multiple of the J_{AF} parameters ($J_{FA1} = 2J_{AF}$ and $J_{FA2} = 0.5J_{AF}$). This methodology is proposed by Kiwi and coauthors [30]. For obtaining J_{FA1} and J_{FA2}, the procedure suggested by Lederman et al. [13] was implemented. It consisted in carrying out hysteresis loops simulation of FM/AF bilayers for different combinations of interface exchange parameters with $J_{FA1} = J_{FA2}$ and $J_{FA1} \neq 2J_{FA2}$, that depends on the AF exchange parameters. Results were compared with experimental reports presented by Campillo et al. [31]. Second and fourth terms account for planar anisotropy for the FM and AF layers, respectively. In this study, $K_F = 1.2484$ meV [18] and $K_A = 2K_F = 2.4968$ meV. The last term accounts for the Zeeman interaction of the spins with a uniform magnetic applied field.

On the other hand, a single-spin movement Metropolis–Monte Carlo algorithm was used for obtaining the equilibrium thermodynamic properties, namely magnetization, energy, specific heat, and magnetic susceptibility. Around 2×10^5 Monte Carlo steps per spin (mcs) were considered and around 1×10^5 mcs were discarded for equilibration. The bilayer construction made by the model is present in Fig. 1. The lower film corresponds to the $La_{2/3}Ca_{1/3}MnO_3$ (FM) layer and the upper film indicates the $La_{1/3}Ca_{2/3}MnO_3$ (AF). This bilayer was built with $L = 30$ lattice parameters, 6 pulses, and 12 relaxation steps. In this image, high roughness is observed.

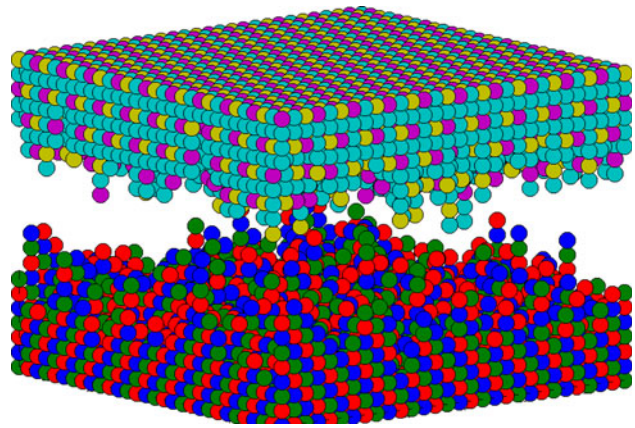

Fig. 1 $La_{2/3}Ca_{1/3}MnO_3/La_{1/3}Ca_{2/3}MnO_3$ bilayer built with $L = 30$ lattice parameters, 6 pulses, and 12 relaxation steps

On the other hand, when the dynamic model of surface height profile is determined, surface roughness of the thin film is defined as the standard deviation of the surface height profile from its average height and is computed as follows

$$R_{ave} = \sum_{n=1}^{N} \frac{|z_n - \bar{z}|}{N} \quad (3)$$

where Z_n is the local height and $\bar{Z}$ is the average surface height. The sum runs over the N positions in the x–y plane [32].

Results and analysis

Figure 2 shows specific heat as a function of the temperature for $La_{1-x}Ca_xMnO_3$ with $x = 1/3$ (FM) and $x = 2/3$ (AF). $T_C \sim 260$ K and $T_N \sim 250$ K can be observed. These values are in agreement with those presented in the

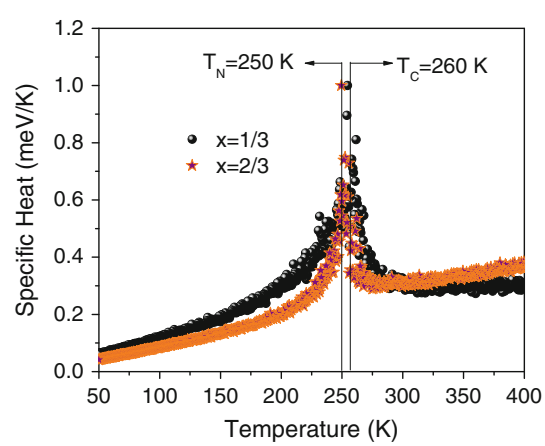

Fig. 2 Temperature dependence of the specific heat for $La_{1-x}Ca_xMnO_3$ with $x = 1/3$ and $x = 2/3$

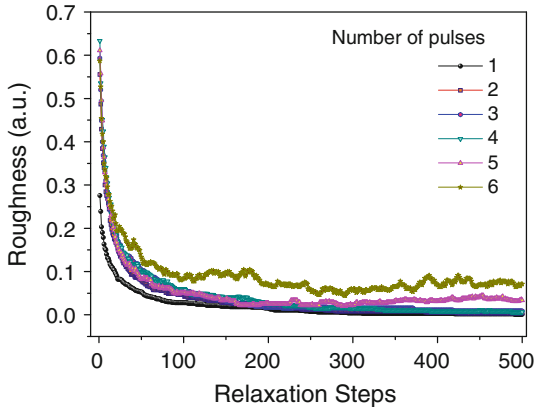

Fig. 3 Relaxation steps dependence of the roughness for different number of pulses. The kinetic roughness behavior is observed

phase diagram reported by several authors [33, 34]. Figure 3 shows relaxation steps dependence of the roughness for different number of pulses. A kinetic roughness behavior is observed, since the roughness varies as a function not only of number of pulses, but also of the relaxation time (Monte Carlo steps). For lower step values (<50), roughness is high. After that, roughness decreases dramatically and tends to be constant. This is an expected behavior, because when the film was grown many high columns of ions were formed. Nevertheless, as the film is relaxed (atoms diffusion), some of these peaks height decreases, and the ions initially placed on the top, fall to lower positions, producing uniformity on the surface. In this study atoms are directed to the surface perpendicularly. During normal angle evaporation, shadowing effect is almost absent. This effect is originated from the preferential deposition of obliquely incident atoms on higher surface points, possibly producing arrays of nanorods and nanosprings, although these nanostructures are not easy to produce, because the majority of processes require high growth temperatures and the use of a metal catalyst [35]. Nevertheless, these nanomaterials have been produced by other methods as vapor liquid solid mechanisms and chemical vapor deposition [35, 36].

When shadowing effect becomes more dominant, films morphology gets more columnar and high degree nodes can exchange atoms with longer distance surface points. Shadowing effect and re-emission process normally compete with local surface diffusion effects [37]. Therefore, in this study we did not include re-emission and shadowing in order to better distinguish the effect of surface diffusion. During the growth, two competing processes play a role in the evolution of the surface morphology (excluding chemical reactions). Firstly, random fluctuations occur all the time resulting in height fluctuations and kinetic roughness build up. Secondly, smoothing effects, such as thermal diffusion or atoms lateral movement, tend to eliminate the height fluctuations. These smoothing effects can only take place at a length scale smaller than or equal to the diffusion length of the add-atoms. The random fluctuations can take place on both, a long as well as short-range scale. As a result, these two processes can only lead to a balancing effect on a relatively short range, and a kinetic roughening of the film will occur [38]. Figure 3 also shows the roughness behavior varying the number of pulses. Roughness increases as the number of pulses increases. An important factor to consider is that the number of pulses is proportional to the thickness, because as the number of ions to be deposited increases, higher peaks are formed. Many studies about the relationship between roughness and thickness are reported in the literature. Salvadori et al. [39] modeled the morphology of $TiSi_2$. The modeling results predicted that the root mean square roughness is essentially linear with film thickness (verified for thickness up to 150 nm). Simulation of film thickness distributed control, surface roughness, and porosity in a porous thin film deposition process is reported by Hu et al. [40]. It is carried out by using the deposition rate as the manipulated input by regulating film surface roughness. It was initially done with desired minimum of film thickness (roughness control problem). They also predict with their simulation an increase in both roughness and thickness as the deposition time increases.

Films morphology also has high influence on important system properties as magnetic behavior. Figure 4 shows the hysteresis loops for different chosen values of relaxation time at a temperature of 200 K and six pulses. The EB phenomenon is observed, and is evident the influence of this parameter on the EB field (H_{ex}) and the coercive field (H_c). Figure 5 shows left, right, and total coercive fields as a function of the relaxation time for six pulses. Many authors report roughness dependence of H_c, and in most of these a direct proportionality is observed as results presented by Palasantzas et al. [41, 42] for Co films deposited

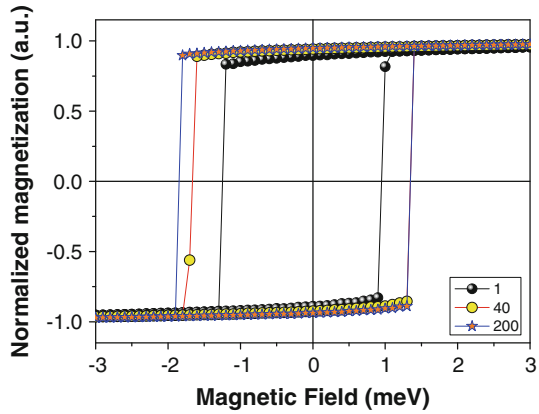

Fig. 4 Hysteresis loops for different chosen values of relaxation time at a temperature of 200 K and six pulses

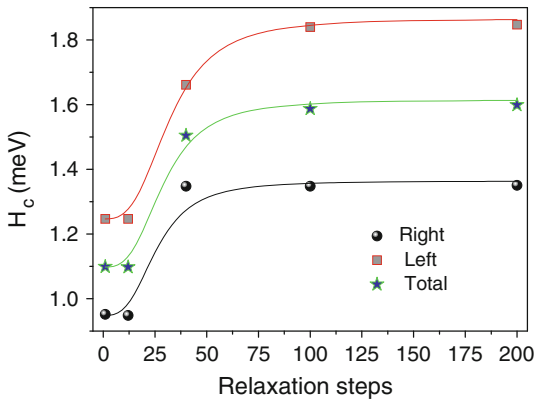

Fig. 5 Left, right, and total coercive fields as a function of the relaxation steps for six pulses

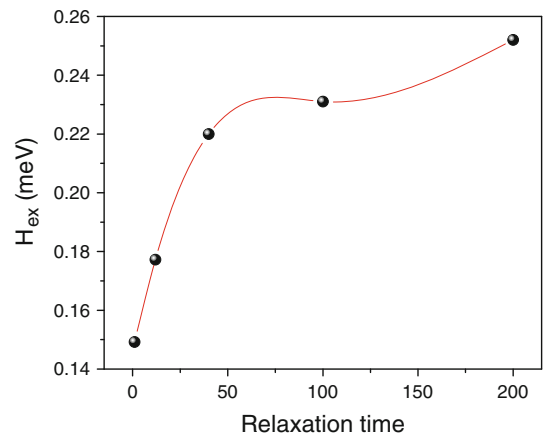

Fig. 6 Relaxation steps dependence of the EB field for six pulses

on Cu substrates. They studied H_c versus roughness and thickness. Initially, H_c increased until a certain value and then it approached saturation as the roughness became higher. Due to the different behavior of magnetic spins in a rough interface, this may be indirectly caused by an increase in interface roughness [43].

The small size of the samples simulated here could not reflect the real behavior of magnetic FM/AF bilayers, and does not allow applying the Neél model when the domain wall width is smaller than the typical length of these surface inhomogeneities and considers a demagnetization effect [44]. According to the results shown in Fig. 3, at lower values of relaxation steps, roughness is high and coercive force is low. However, as the roughness decreases (increasing relaxation steps), coercive force increases. Finally, when roughness reaches the saturation at lower values, H_c also reaches a maximum and then it is saturated. It could be due to the spins disorder at the interface helps the demagnetization effect, decreasing the coercive force needed for reaching zero magnetization. As the roughness decreases, the spin disorder tends to disappear, and H_c reaches the value for a flat surface. Figure 6 presents the relaxation steps dependence of the EB for six pulses. Results such as decreased short-range roughness in the $La_{2/3}Ca_{1/3}MnO_3/La_{2/3}Ca_{1/3}MnO_3$ interface leads to an increase in the exchange biasing field H_{ex}. Most investigations of the roughness role on EB in thin films seem to agree that the magnitude of H_{ex} decreases with increasing roughness [45–47]. The roughness creates areas of different spin orientations, thus the total number of spins pinning the FM in one direction is reduced, concomitantly reducing the magnitude of H_{ex}. More sophisticated models assume that roughness affects the interface coupling, J_{INT}, and consequently the magnitude of H_{ex} [48, 49]. Finally, roughness may affect the formation of domains (e.g., by pinning) in the AF layer or the amount of uncompensated surface spins and thus influence H_{ex} [50]. According to the random-field model of exchange biasing proposed by Malozemoff [51], the H_{ex} arises from average random-field energy per area $\Delta\sigma = f_i J/aL$ and can be expressed as follows

$$H_{EB} \propto \frac{\Delta\sigma}{2M_f d_{FM}} \propto \frac{f_i J}{2M_f d_{FM} aL} \quad (4)$$

where M_f and d_{FM} are the magnetization and thickness of the ferromagnet, respectively, f_i is a parameter related to randomness of spin orientations with order unity, J is the atomic interfacial exchange coupling (in this case J_{FA1} and J_{FA2}), a is the atomic spacing, and L is the domain size.

Conclusions

Influence of roughness in EB and coercive field for FM/AF bilayers was studied, grown by using the Monte Carlo method. Roughness was related to the relaxation steps decreasing as the film was relaxed. Moreover, H_{ex} and H_c are inversely related to the roughness.

Acknowledgements The authors gratefully acknowledge the financial support of la Dirección Nacional de Investigaciones during the course of this research, under Project 7785. This study was also supported in part by the GES and GICM Sustainability projects and the IN565CE project of the Antioquia University.

References

1. Stout KJ, Blunt L (1995) Surf Coat Technol 71:69
2. Adamson AW, Gast AP (1997) Physical chemistry of surfaces, 6th edn. Wiley-Interscience, New York
3. Bhushan B (1998) Tribol Lett 4:1
4. Poon CY, Bhushan B (1995) Wear 190:76
5. Bland JAC, Heinrich B (eds) (1994) Ultrathin magnetic structures I and II. Springer, New York
6. Tien CL, Yang HM, Liu MC (2009) Thin Solid Films 517:5110
7. Kools JCS (1996) IEEE Trans Magn 32:3165
8. Engel BN et al (2005) IEEE Trans Magn 41:132

9. Parkin SSP, Jiang X, Kaiser C, Panchula A, Roche K, Samant M (2003) Proc IEEE 91:660
10. Rojas Sánchez JC, Granada M, Steren LB, Mazzaro I, Mosca DH (2007) Appl Surf Sci 254:219
11. Liu C, Yu C, Jiang H, Shen L, Alexander C (2000) J Appl Phys 87:6644
12. Nogués J, Moran TJ, Lederman D, Schuller IK, Rao KV (1999) Phys Rev B 59:6984
13. Lederman D, Nogués J, Schuller IK (1997) Phys Rev B 56:2332
14. Nogues J, Lederman D, Schuller IK (1996) Appl Phys Lett 68:3186
15. Nascimento VP, Passamani EC, Alvarenga AD, Pelegrini F, Biondo A, Baggio E (2008) J Magn Magn Mater 320:e272
16. Uyama H, Otani Y, Fukamichi K, Iwasaky H, Sahashi M (1997) J Magn Soc Jpn 21:911
17. Han DH, Zhu JG, Judy JH (1997) J Appl Phys 81:4996
18. Zeng Z, Udpa L, Udpa SS (2006) IEEE Trans Magn 42:10
19. Christides C, Deen PP, Moutis N, Houssakou E, Bouchenoire L, Prassides K (2007) Phys Rev B 75:014432.1
20. Cotton FA (1990) Chemical applications of group theory, 3rd edn. Wiley, New York
21. Hotta T, Feiguin A, Dagotto E (2001) Phys Rev Lett 86:4922
22. Hotta T, Malvezzi AL, Dagotto E (2000) Phys Rev B 62:9432
23. Nachev IS (1995) J Phys Chem Solids 56:1039
24. Landau DP, Binder K (2005) A guide to Monte Carlo simulations in statistical physics, 2nd edn. Cambridge University Press, Cambridge, MA
25. Cho J, Terry SG, LeSar R, Levi CG (2005) Mater Sci Eng A 39:390
26. Zener C (1951) Phys Rev 81:440
27. Bao W, Axe JD, Chen CH, Cheong S-W, Schiffer P, Roy M (1998) Physica B 241–242:418
28. Restrepo-Parra E, Restrepo J, Jurado JF, Vargas-Hernández C, Riaño-Rojas JC (2009) IEEE Trans Magn 45:5180
29. Riaño-Rojas JC, Restrepo-Parra E, Orozco-Hernández G, Restrepo J, Jurado JF, Vargas-Hernández C (2009) IEEE Trans Magn 45:5196
30. Lederman D, Ramírez R, Kiwi M (2004) Phys Rev B 70:184422
31. Campillo G, Hoffmann A, Gómez ME, Prieto P (2005) Rev Col Phys 37:215
32. Riaño-Rojas JC, Restrepo-Parra E, Prieto-Ortiz FA, Olaya JJ (2006) Rev Col Fis 38:39 (in spanish)
33. Cheong S-W, Hwang HY (1999) In: Tokura Y (ed) Ferromagnetism versus charge/orbital ordering in mixed valent manganites in colossal magnetoresistance oxides. Gordon and Breach Monographs in Condensed Matter Science, London
34. Yoo Y-K, Duewer F, Yang H, Yi D, Li J-W, Xiang XD (2000) Nature 406:704
35. Wang L, Major D, Paga P, Zhang D, Norton MG, Mcllroy DN (2006) Nanotechnology 17:S298
36. Wagner R, Ellis W (1964) Appl Phys Lett 4:89
37. Karabacak T, Guclu H, Yuksel M (2009) Phys Rev B 79:195418
38. Amorsolo AV, Funkenbusch PD, Kadin AM (1999) Mater Sci Eng B57:186
39. Salvadori MC, Martins DR, Cattani M (2006) Surf Coat Technol 200:5119
40. Hu G, Orkoulas G, Christofides PD (2009) Chem Eng Sci 64:3903
41. Palasantzas G, Zhao Y-P, De Hosson JThM, Wang G-C (2000) Physica B 283:199
42. Palasantzas G (2005) Phys Rev B 75:205320
43. Kirilyuk A, Rasing Th, Haast MAM, Lodder JC (1998) Appl Phys Lett 72:2331
44. Zhang J, White RM (1996) IEEE Trans Magn 32:4630
45. Shen JX, Kief MT (1996) J Appl Phys 79:5008
46. Park CM, Min KI, Shin KH (1996) J Appl Phys 79:6228
47. Soeya S, Fuyama M, Tadokoro S, Imagawa T (1996) J Appl Phys 79:1604
48. Mauri D, Siegmann HC, Bagus PS, Kay E (1987) J Appl Phys 62:3047
49. Neel L (1967) Ann Phys 1:61
50. Takano K, Kodama RH, Berkowitz AE, Cao W, Thomas G (1997) Phys Rev Lett 79:1130
51. Malozemoff AP (1988) J Appl Phys 63:3874